

# EMBANKMENT BREACH RESEARCH: OBSERVED INTERNAL EROSION PROCESSES

A. K. Ali, S. L. Hunt, R. D. Tejral



## HIGHLIGHTS

- This study provides data from internal erosion tests on four intermediate-scale homogeneous embankment dams.
- Soil properties influence the breach formation process and breach timing.
- Results showed that observed erosion rates of the internal flow path varied by several orders of magnitude.
- Quality control of embankment construction can greatly influence breach development.

**ABSTRACT.** Internal erosion and embankment overtopping are the two most common causes of embankment dam and levee failures and incidents. Internal erosion is the removal of soil material by the flow of water through a continuous defect, cavity, or crack within a compacted fill and/or its foundation. Internal erosion initiates from vulnerabilities within the embankment. The embankment soil material plays a key role in both the erosion process and rate of failure, but characterizing soil properties and how they relate to the rate of failure can be challenging. Soil properties such as texture, density, strength, moisture content, and erodibility can vary greatly; thus, it is important to study the effects of these properties on the breach formation process and breach timing. The USDA Agricultural Research Service performed internal erosion breach experiments on four intermediate-scale homogeneous earthen embankments constructed of soils ranging from a silty sand to a lean clay material. The embankments were constructed to a height of 1.3 m, a top width of 1.8 m, and upstream and downstream slopes of 3(H):1(V). The embankment materials were characterized by water content, density, texture, strength, and erodibility. Erodibility was measured using a jet erosion test (JET) apparatus. A 40 mm diameter, continuous steel pipe was placed through each embankment during construction and removed to form an open-ended void through the embankment connected to the upstream reservoir. The removal of the pipe initiated internal erosion. The objectives of the experiments were to observe the development of the internal erosion process over time and to examine the influence of soil properties on the erosion rate, breach timing, geometry of the breach opening, and breach outflow. The rate of erosion and failure observed in these tests varied by several orders of magnitude, with the silty sand embankment eroding most rapidly and the lean clay embankment with a mean moisture content of 18% dry basis at standard compaction eroding the slowest. These observations were indicative of the soil textures. Although the two lean clay embankments were constructed of similar soils, the difference in erosion rates speak to the importance of quality control (e.g., compaction moisture content) during construction. Soil properties including soil texture, erodibility, and compaction moisture content are key predictors of erosion rate and observed failure.

**Keywords.** Breach, Dam failure, Dams, Embankments, Erodibility, Internal erosion, Levees, Overtopping

**S**tories of catastrophic floods, such as those created by major hurricanes Harvey, Irma, and Maria in 2017 and Florence in 2018 and events that led to the 2017 Oroville Dam incident in California and the

---

Submitted for review on 25 September 2019 as manuscript number NRES 13701; approved for publication as a Research Article by the Natural Resources & Environmental Systems Community of ASABE on 20 November 2020.

Mention of company or trade names is for description only and does not imply endorsement by the USDA. The USDA is an equal opportunity provider and employer.

The authors are **Abdelfatah K. Ali**, ORAU/ORISE Postdoctoral Research Associate, and **Sherry L. Hunt**, Supervisory Civil Engineer, USDA-ARS Hydraulic Engineering Research Unit, Stillwater, Oklahoma; **Ronald D. Tejral**, Engineer, Nebraska Public Power District, North Platte, Nebraska. **Corresponding author:** Abdelfatah Ali, USDA-ARS, 1301 N. Western Rd., Stillwater, OK 74075; phone: 405-385-5474; e-mail: abdelfatah.ali@usda.gov.

2019 Spencer Dam failure in Nebraska, have dominated headline news in recent years. Flood damages and dam failures like these have skyrocketing economic impacts. For example, Dunker (2019) reported that flooding in Nebraska in early 2019 caused \$1.3 billion in damages (\$1 billion to agriculture) and disrupted travel on about 2,000 miles of state roads. Floods like these place stress on dams, and while dams across the U.S. have had an excellent safety record, dams do fail, placing life and property downstream at potential risk. According to the National Performance of Dams Program (NPD, 2018), approximately 4% of the dam failures in the U.S. have caused fatalities.

Incidents such as these have brought both national and worldwide attention to the need to improve dam breach prediction tools and flood warning systems. Dam breach prediction tools may provide ways to enhance emergency action plans should a dam incident occur, inform policymakers

responsible for setting zoning regulations, and assist in the prioritization of rehabilitation for aging dams.

The USDA Natural Resources Conservation Service (NRCS) has provided both technical and financial assistance for the construction of nearly 12,000 flood control dams in small watersheds through the Small Watershed Program (Hanson et al., 2007). However, by 2017, half of these dams had reached the end of their planned service life. While many of these dams have performed well and as intended, some are in need of modification. Reservoirs have filled with sediment, and demographic changes have increased the downstream hazard potential (e.g., low hazard with impact to agricultural resources increasing to high hazard with potential loss of human life). Changes in hazard classification require dams to meet more stringent design criteria, and spillway capacity is often inadequate to pass the required storm event.

For the past two decades, scientists at the USDA Agricultural Research Service (ARS) Hydraulic Engineering Research Unit (HERU) have performed research to address the rehabilitation of small watershed flood control structures and develop engineering tools to examine dam breach potential due to overtopping (Hanson and Temple, 2002; Hanson and Cook, 2004; Hanson et al., 2005, 2010a, 2010b, 2011; Hunt et al., 2005; Hanson and Hunt, 2007). Hanson et al. (2010a) expanded that research to examine dam breaches caused by internal erosion, reporting details from two of four homogeneous embankment breach tests performed at the HERU. This article expands upon that work by describing the detailed observations made during all four tests.

## BACKGROUND

Foster et al. (2000) conducted a statistical analysis on an extensive database of dam failures and concluded that piping and overtopping were the primary modes of embankment failure, with each accounting for about 40% to 50% of all dam failures. Numerous embankment overtopping studies, exist ranging from small-scale (Hassan et al., 2004; Tabrizi et al., 2017) to intermediate-scale (Hanson et al., 2005, 2010a) to large-scale embankments (Vaskinn et al., 2004; Zhong et al., 2019). In addition to those studies, supporting research has been conducted on vegetal slope protection (Hanson and Temple, 2002), rock slope protection (Abt and Johnson, 1991; Frizzell et al., 1998; Mishra and Ruff, 1998; Robinson et al., 1998), material characterization (Hanson and Hunt 2007; Hanson et al. 2011), and breach widening processes (Hunt et al., 2005).

While those previous studies have improved our knowledge of overtopping breach processes, understanding the processes involved in the failure of embankments due to piping has been more challenging due to the difficulty in making observations, collecting data, and distinguishing between the processes involved. Wilson and Fox (2013) even discussed confusion with the terminology used by various disciplines to describe piping and internal erosion process, e.g., "heave (boil), sapping, backwards erosion, seepage erosion, tunneling (or jugging), suffusion, pipeflow, and internal erosion." They discussed how internal erosion is often

used to describe translocation of fines through an earthen embankment (ASCE Task Committee on Dam/Levee Breaching, 2011). However, flow through a discrete conduit (soil pipe) or linear void, as described by Bernatek-Jakiel and Poesen (2018), is a distinct form of piping (Wilson, 2011). There is some consensus that internal erosion involves flow through a linear void (soil pipe, crack, etc.) at a sufficient rate to erode the inside walls of the void (Hanson et al., 2010a; Wilson, 2011; Wilson and Fox, 2013). This is in contrast to suffusion, which involves seepage forces moving fines through permeable zones of the soil or embankment, ultimately leading to the creation of a linear void. This distinction avoids the confusion of internal erosion with suffusion, or rather the lumping of these distinct yet interacting piping processes. Fell et al. (2003) identified four phases of embankment failure: initiation, continuation, progression, and breaching. The initiation and continuation of internal erosion in embankments is further described as occurring through the following mechanisms: backward erosion, crack or hydraulic fracture, high-permeability zone, and suffusion or internal instability.

Hanson et al. (2010a) identified inadequate compaction during construction, differential settlement, desiccation, earthquakes, burrowing animals, and/or decay of roots as other causes that create cavities or voids, in addition to suffusion. Given the role of these structural defects in initiating the formation of voids, the ASCE Task Committee on Dam/Levee Breaching (2011) and Costa (1985) included structural defects as a separate category of dam failure causes, in addition to piping and overtopping. An example of a such a failure event is shown in figure 1, where preferential flow along the principal spillway pipe caused internal erosion of the void.

Fell et al. (2003) discussed several factors within an embankment that can influence the likelihood of flow path enlargement by erosion, including hydraulic gradient, soil type, clay fraction, dispersion, compaction water content and density, and degree of saturation. Fell et al. (2003) and McCook (2004) identified soil erodibility and hydraulic stress along the internal erosion path as the most likely influences on the rate of erosion during internal embankment breach development.

Intermediate-scale to large-scale internal erosion studies on embankment dams that have provided some limited data include those by Fell et al. (2003), Vaskinn et al. (2004), Hanson et al. (2010a), and Wahl and Lentz (2011). Moglen et al. (2018) provided a database of studies and real-world dam failures, but very few if any of the studies provided detailed data related to dam failures caused by internal erosion. Many of the studies outlined above highlighted soil parameters, including soil erodibility, compaction effort, soil moisture content, and soil texture, as the greatest influences on embankment dam erosion processes and failure. Hanson et al. (2010a) stated that in order for a failure to occur from internal erosion or overtopping, three conditions must be met: (1) there must be an existing flow path, (2) there must be a source of water, and (3) the hydraulic stresses must be great enough to cause detachment of material. Hanson et al. (2010a) also indicated that all soils are susceptible to erosion to some degree; therefore, the soil must be evaluated to



Figure 1. Internal erosion initiated along the principal spillway pipe of Upper Red Rock Site 20 in Oklahoma.

determine its erodibility. Sherard et al. (1972) and McCook (2004) identified problematic soils (e.g., dispersive clays, low-plasticity silts, and sands with significant fines) used in dam construction that are more vulnerable to erosion than others.

While studies on internal erosion through earthen embankments are limited, many *in situ* studies have been conducted on these processes (Bernatek-Jakiel and Poesen, 2018). In addition, numerous mechanistic and empirical studies on internal erosion by pipeflow have been conducted under controlled laboratory conditions (Wilson, 2009, 2011; Fox et al., 2014; Robbins and Griffiths, 2018; Wanger et al., 2019) and even under controlled field conditions (Midgley et al., 2013). Wilson (2009) created artificial soil pipes in laboratory flumes oriented at a 15% slope by packing soil around a 1 cm diameter rod that extended the length of the soil bed. The soils for these experiments were described as a 5 cm thick layer of silty clay loam, representing a water-restrictive layer, and an upper 10 cm thick layer of soil described as Providence silt loam packed on top of the silty clay loam. The placement of the rod was just above the water-restrictive soil layer. After pulling the rod out at the lower end to create an artificial soil pipe, the upper end was connected to a water inflow port, and flow was established at a steady rate. Wilson (2009) found that despite the constant inflow, pipeflow was highly unstable due to internal mass wasting temporarily clogging the pipe, followed by surges in pipeflow with high sediment fluxes. Wilson (2009) used combined features of the Slot Erosion Test (SET) developed by Wan and Fell (2004) and the Hole Erosion Test (HET) to determine the critical shear and soil erodibility for internal erosion in the soil pipe. He reported that the application of the SET and HET methods for internal erosion of the soil pipe at a constant flow rate had limited success, and improved methods are needed for measuring the internal dimensions of soil pipe enlargement to accurately determine critical shear stress and erodibility coefficients.

Wilson (2011) repeated the Wilson (2009) studies for a range of initial pipe sizes (2 to 10 mm i.d.) using a constant head of 15 cm to simulate conditions in which the soil pipe is open to a water reservoir. Several modifications to the

experiment were made in an attempt to determine what boundary condition best represented pipe flow. Additionally, another test was conducted on Smithdale loam. Wilson (2011) again found extremely erratic flow rates and sediment concentrations as the soil pipe temporarily clogged and then reopened, and he observed rapid tunnel collapse (within minutes) for most conditions tested. Wilson and Fox (2013) applied a Richards equation approach to modeling the data obtained by Wilson (2009, 2011) and observed that extreme pressure jumps occurred in less than 0.1 s over several meters using a constant flux boundary condition and over several centimeters using a constant head boundary condition within soil pipes when the pipes clogged due to mass wasting of the pipe walls.

Fox et al. (2014) also studied internal erosion processes in small laboratory soil beds to evaluate mechanistic models for soil piping. Discrepancies between observed and predicted sediment concentrations were noted for cases with highly erodible soils, and in many cases the soil pipe eroded so quickly that transport-limited conditions were created, leading to pipe clogging similar to that observed by Wilson (2009, 2011). Fox et al. (2014) corroborated the findings of Wilson and Fox (2013) by indicating that this clogging can lead to buildup of pore water pressures that can cause catastrophic failure. In addition, Fox et al. (2014) observed that simple geometries, such as those assumed for the model, were not represented in all cases due to material quickly eroding and the soil pipe expanding preferentially at the bottom of the pipe cross-section. Fox et al. (2014) recommended additional research to observe soil piping and internal erosion through various soil pipe sizes, shapes, and path lengths. In their review of internal erosion of soil pipes, Wilson et al. (2018) made several recommendations for future mechanistic research that would lead to the development of models capable of simulating sediment detachment and transport (i.e., internal erosion) in soil pipes.

This study addresses in part the research needs outlined by Wilson et al. (2018) but is specifically focused on embankment failure scenarios. The objective of this study is to observe embankment internal erosion processes for the improvement of computational models for predicting embankment failure, so that (1) aging embankment dams can be prioritized for rehabilitation, (2) improved dam failure warning systems can be developed, (3) policymakers can be informed for developing zoning regulations in the vicinity of dams, and (4) emergency managers can have better tools for emergency action planning. While algorithms quantifying the dominant processes of breach erosion and predictive computational models, such as the National Weather Service (NWS) Breach model (Fread, 1988), Windows Dam Analysis Modules (WinDAM) B model (Hanson et al., 2011), the Center for Computational Hydroscience and Engineering (CCHE) two-dimensional (2D) model (Jia and Hunt, 2016), and the Nanjing Hydraulic Research Institute (NHRI) model (Zhong et al., 2019), have been developed, those models and algorithms primarily apply to the breach processes associated with embankment overtopping. This study provides the basis for enhancement of those tools to include internal erosion.

## EROSION PROCESS ALGORITHMS

Soil erodibility was identified by Hanson et al. (2007, 2010a, 2010b) and Zhong et al. (2019) as key to the breach timing, breach outflow, and failure probability of embankment dams. Soil erodibility is most commonly described in the literature by the excess stress equation (Temple, 1985; Fell et al., 2003; Zhong et al., 2019). The excess stress equation on a volume per unit of time basis is as follows:

$$E_r = k_d (\tau_e - \tau_c)^a \quad (1)$$

where

$E_r$  = rate of erosion ( $\text{m s}^{-1}$ )

$k_d$  = detachment/erodibility coefficient ( $\text{m}^3 \text{N}^{-1} \text{s}^{-1}$ )

$\tau_e$  = effective stress/hydraulic stress ( $\text{N m}^{-2}$ )

$\tau_c$  = critical stress ( $\text{N m}^{-2}$ )

$a$  = exponent (assumed = 1).

Note that  $k_d$  is most commonly reported in units of  $\text{cm}^3 \text{N}^{-1} \text{s}^{-1}$ , so a conversion is often necessary in the application of equation 1.

The excess stress on a mass per unit of time can be defined by a similar expression:

$$E_c = C_e (\tau_e - \tau_c)^a \quad (2)$$

where

$E_c$  = rate of erosion in ( $\text{kg s}^{-1} \text{m}^{-2}$ )

$C_e$  = detachment/erodibility coefficient ( $\text{s m}^{-1}$ ;  $C_e = k_d \rho$ , where  $\rho$  is dry density ( $\text{kg m}^{-3}$ )).

For the purposes of internal erosion analysis, the effective stress on the boundary can be approximated as the gross or total boundary stress and can be computed as:

$$\tau_e = \gamma R (H_L / L) \quad (3)$$

where

$\gamma$  = unit weight of water ( $\text{N m}^{-3}$ )

$R$  = hydraulic radius of the pipe = area/wetted perimeter (m)

$H_L$  = frictional energy loss (m)

$L$  = length of pipe over which frictional energy loss ( $H_L$ ) occurs (m).

The soil erodibility coefficient as reported by Hanson and Cook (2004) has been observed to range over several orders of magnitude. For example, a value of  $0.001 \text{ cm}^3 \text{ N}^{-1} \text{s}^{-1}$  is associated with very erosion-resistant soil materials, whereas a value of  $1000 \text{ cm}^3 \text{ N}^{-1} \text{s}^{-1}$  indicates a highly erodible soil material.

Because the erodibility coefficient ( $k_d$ ) can vary over several orders of magnitude, Hanson et al. (2010a) developed

table 1 based on the erodibility classification system proposed by Wan and Fell (2004). According to Hanson et al. (2010a), this classification system describes the erosion resistance of soils by assigning a group number (i.e., 1 to 6), with larger numbers indicating increasing erosion resistance linked to the erosion rate index ( $I$ ), which is defined as  $-\log(C_e)$ , and qualitative description of the erosion resistance. Hanson et al. (2010a) enhanced the classification system proposed by Wan and Fell (2004) by adding  $k_d$  and  $C_e$  in correspondence with the erosion rate index, group number, and qualitative description of the erosion resistance. Soils more erodible than  $k_d = 33 \text{ cm}^3 \text{ N}^{-1} \text{s}^{-1}$  and  $C_e = 0.05 \text{ s m}^{-1}$  are designated as group 1, and their erosion is described as extremely rapid.

Testing methods such as flume tests, the jet erosion test (JET), and the hole erosion test (HET) are often used to assess the erosion rates of soils. While flume tests have proven useful in studying erosion processes and rates, this testing procedure poses problems when evaluating soils in their existing environment (i.e., streambed, streambank, constructed dams and levees, etc.). To address the need to determine erosion rates and soil erodibility parameters *in situ* as well as in laboratory settings, Hanson and Cook (2004) developed the JET apparatus and testing procedures. The JET analysis results provide an estimate of two soil parameters, soil erodibility ( $k_d$ ) and critical shear stress ( $\tau_c$ ), that may be applied directly in equation 1. Conversion of  $k_d$  from the JET results to  $C_e$  allows application in equation 2. Wan and Fell (2004) developed the HET to provide a laboratory measurement of the soil parameters  $C_e$  and  $\tau_c$  that may be applied directly in equation 2. Likewise, conversion of  $C_e$  from the HET results to  $k_d$  allows application in equation 1.

## EXPERIMENTAL SETUP

### EMBANKMENT TEST

Four intermediate-scale physical models of homogeneous earthen embankments were constructed and tested at the HERU to simulate internal erosion and associated breach development. Two of these tests were previously reported by Hanson et al. (2010a); this article provides results from all four tests. The purposes of these tests were to observe erosion processes and to determine the impact of soil properties on the erosion rate, the timing and geometry of an embankment breach, and the outflow hydrograph. The test embankments were constructed with compacted lift thicknesses of about 0.11 m to a height of 1.3 m (fig. 2). Compaction was achieved using a self-propelled vibratory pad-foot roller, with each lift compacted with two passes of the roller in vibration mode. The top widths of the finished embankments

**Table 1. Relationship of  $k_d$ ,  $C_e$ ,  $I$ , group number, and qualitative erosion resistance (after Hanson et al., 2010a).**

$k_d$ ( $\text{cm}^3 \text{N}^{-1} \text{s}^{-1}$ )	$C_e$ ( $\text{s m}^{-1}$ ) <sup>[a]</sup>	$I$ ( $-\log(C_e)$ ) <sup>[a]</sup>	Group Number <sup>[b]</sup>	Qualitative Description <sup>[b]</sup>
33	0.05 to 0.07	1.2 to 1.3	1	Extremely rapid
3.3	0.005 to 0.007	2.2 to 2.3	2	Very rapid
0.33	0.0005 to 0.0007	3.2 to 3.3	3	Moderately rapid
0.033	0.00005 to 0.00007	4.2 to 4.3	4	Moderately slow
0.0033	0.000005 to 0.000007	5.2 to 5.3	5	Very slow
0.00033	0.000005 to 0.000007	6.2 to 6.3	6	Extremely slow

<sup>[a]</sup> Based on a range of dry density ( $\rho$ ) values from 1500 to 2000  $\text{kg m}^{-3}$ .

<sup>[b]</sup> Groupings and qualitative descriptions are based on Wan and Fell (2004).

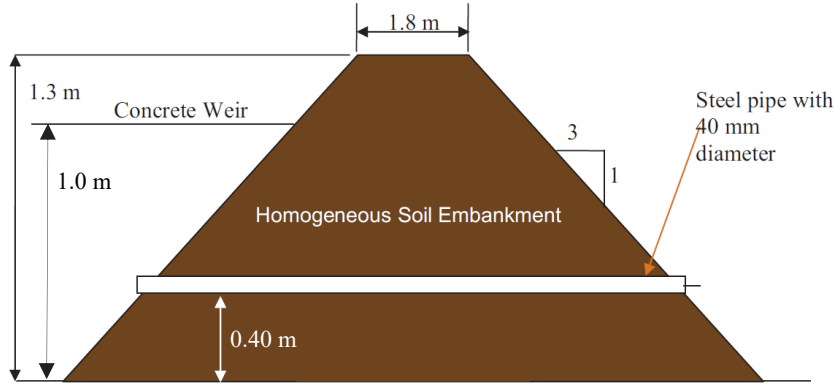


**Figure 2.** Schematic of embankment for internal erosion tests (not to scale) (after Hanson et al., 2010a).

were 1.8 m, and the upstream and downstream slopes were 3(H):1(V). A 40 mm diameter continuous steel pipe was placed through the embankment at an approximate height of 0.40 m above the base of the dam. The upstream end of the pipe was capped to prevent flow from entering the embankment during reservoir filling. After filling, the steel pipe was removed by pulling it out of the downstream face of the embankment to initiate internal erosion (Hanson et al., 2010a).

Five siphons connected to the adjacent Lake Carl Blackwell provided the water source for the tests. Flow was released from the siphons and delivered to the upstream reservoir through a network of channels on the laboratory grounds. Inflow to the upstream reservoir was monitored over a sharp-crested weir with a combination of a gauge well, a point gauge, and a chart recorder fitted with a digital encoder. As described by Hanson et al. (2010a), flow was allowed to pass through the embankment opening after removal of the steel pipe (fig. 2) and/or pass over a 43 m long side weir located upstream of the embankment (fig. 3) during the initial stages of the internal erosion process. The height of the side weir above the base of the dam was approximately 1.0 m. The side weir allowed a relatively constant elevation to be maintained in the upstream pool during the early internal erosion stages of the test and simulated a large reservoir upstream of the test embankment. In later stages of the erosion process, the reservoir head decreased, resulting in collapse of the top of the embankment dam. Staff gauges, point gauges, chart recorders, and digital encoders were used to track reservoir and tailwater elevations. Reservoir elevations were used to determine the storage volume in the reservoir

during the test and to determine the discharge over the side weir. Reservoir stage-storage relationships were developed using a topographic survey of the reservoir storage volume for verification. Outflow hydrographs were determined by evaluating the inflow, change in storage, and flow over the side weir. Tailwater elevations were measured using a digital encoder and a manually operated point gauge mounted to a chart recorder located approximately 65 m downstream of the embankment toe. When tailwater was not of sufficient depth to be recorded by the digital encoder or manually operated point gauge, tailwater data were estimated from water surface elevations measured downstream of the embankment and from review of digital photographs.

Digital photography and videography documented observations including test initiation, erosion development of the soil pipe, collapse of the top of dam, and the continuation of erosion development through breach widening. The embankments were marked with crosshairs using athletic field chalk that provided a means for calibrating erosion width measurements from the digital photographs. As described by Hanson et al. (2005), an overhead rolling carriage with a manually operated point gauge was used to obtain centerline and cross-sectional bed elevations and water surface elevations during testing.

## SOIL MATERIALS

For the construction of the four embankments, three homogeneous soil materials were used. Table 2 provides a description of the soil materials used for each test, including the soil classification, particle size distribution, and plasticity index (PI). Although table 2 shows slight differences in the soil properties for tests P3 and P4, the soil for these test embankments was obtained from a single borrow pit. Therefore, the embankments for these tests may be considered to have been constructed from essentially the same material. In the laboratory, test samples for each of the soils were prepared at standard compaction effort over a range of water contents. Figure 4 shows the laboratory compaction curves for the three soils under standard compaction conditions. Figure 4 also shows the average compacted water content and average dry bulk density for samples taken during construction of the four embankments. The average compacted moisture content from the construction lifts for the four tests ranged from 11.2% to 17.5%. The average dry bulk density for the four embankments ranged from 1.7 to 1.8 g cm<sup>-3</sup>.



**Figure 3.** Weir upstream of embankment (after Hanson et al., 2010a).

**Table 2. Soil properties.**

Test	Soil Classification <sup>[a]</sup>	Sand <sup>[a]</sup>	Fines <sup>[a]</sup>	Fines <sup>[a]</sup>	PI <sup>[b]</sup>
		>75 µm (%)	>2 µm (%)	<2 µm (%)	
P1	Silty sand	74	20	6	NP
P2	Silt	32	52	15	3
P3	Lean clay	20	54	26	15
P4	Lean clay	13	60	27	15

[a] Based on ASTM Standard D2487 (ASTM, 2000a).

[b] Based on ASTM Standard D4318 (ASTM, 2000b);

PI = plasticity index, and NP = non-plastic.

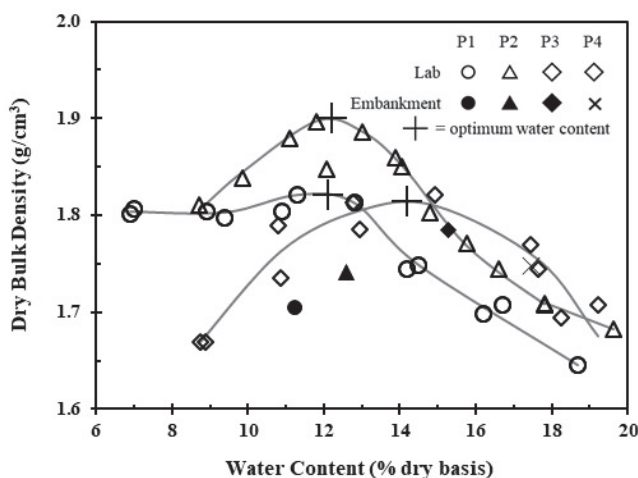


Figure 4. Mean dry bulk density versus mean water content (% dry basis) at standard compaction for embankment construction materials for each test with laboratory standard compaction curves.

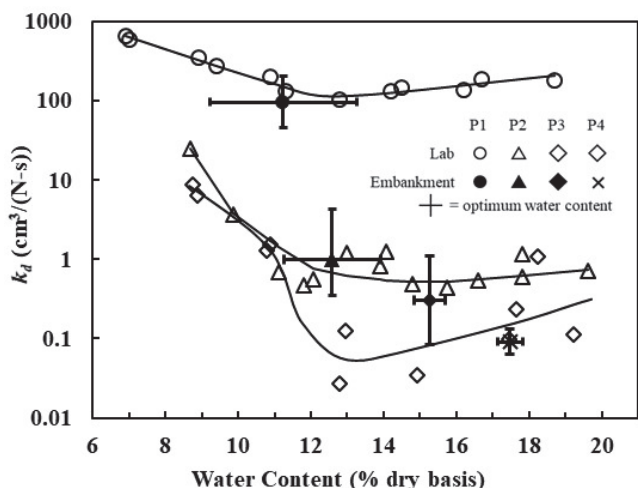


Figure 5. Post-breach mean erodibility ( $k_d$ ) versus mean construction water content (% dry basis) at standard compaction for each embankment with 95% confidence intervals and laboratory erodibility curves at standard compaction.

Laboratory JETs were conducted to characterize the differences in erodibility of the soil materials used for each test over a range of water contents at standard compaction effort. The  $k_d$  value was determined using the JET methodology described by Hanson and Cook (2004). Figure 5 shows the laboratory erodibility curves for the three soils under standard compaction conditions and the average erodibility from undisturbed samples and *in situ* tests taken during embankment construction. The graph of compaction water content versus  $k_d$  provides valuable information about the relative

erodibility of the three materials and the impact of placement water contents. It is apparent that the soils in embankments P3 and P4 were several orders of magnitude more erosion-resistant than the soil in embankment P1. The silty sand material (P1) had a measured  $k_d$  value of  $100 \text{ cm}^3 \text{ N}^{-1} \text{ s}^{-1}$  compacted near optimum water content, and according to table 1, a soil with a  $k_d$  value of  $100 \text{ cm}^3 \text{ N}^{-1} \text{ s}^{-1}$  would be expected to exhibit extremely rapid erosion. As shown in figure 5, the soils in embankments P3 and P4 had measured average embankment  $k_d$  values ranging from  $0.09 \text{ cm}^3 \text{ N}^{-1} \text{ s}^{-1}$  (P4) to  $0.3 \text{ cm}^3 \text{ N}^{-1} \text{ s}^{-1}$  (P3) and were wet of optimum water content. Table 1 indicates that the P4 soil should have exhibited a moderately slow erosion progression, and the P3 soil was closer to a moderately rapid erosion progression.

## TEST RESULTS AND OBSERVATIONS

Figures 6 through 9 illustrate the observed erosion processes during each of the tests. Once the reservoir was filled and water was flowing over the long weir on the upstream side of the test embankment, the 40 mm diameter pipe was pulled out of the embankment and testing was initiated. As noted by Hanson et al. (2010a), rapid erosion for test P1 was expected, given that the soil erodibility was greater than  $33 \text{ cm}^3 \text{ N}^{-1} \text{ s}^{-1}$ , which categorizes it in group 1 in table 1.

Figures 6a to 6f illustrate the progression of erosion during the P1 test. The flow path enlarged rapidly on the downstream side, and the top of the dam collapsed within 14 min of test initiation. Once collapse occurred, breach widening developed at a rapid pace (Hanson et al., 2010a). The breach widening mimicked stage IV of the erosion breach process described by Hunt et al. (2005). Additionally, as noted by Hanson et al. (2010a), in the early stages (fig. 6b) of the internal erosion process, a headcut developed at the flow outlet and progressed rapidly upstream. For embankment P1, the post-breach soil erodibility range from the *in situ* tests on the embankment and undisturbed samples was  $23 \text{ cm}^3 \text{ N}^{-1} \text{ s}^{-1} \leq k_d \leq 270 \text{ cm}^3 \text{ N}^{-1} \text{ s}^{-1}$ . The lower post-breach erodibilities may be attributed to samples taken and/or *in situ* testing conducted near the non-erodible boundary placed at each end of the embankment for protection of the carriage system, whereas higher values of erodibility are more indicative of the soil used in embankment construction. Regardless, as shown in figure 5, the average  $k_d$  was consistent with the standard erodibility curve. Figure 5 also shows that the soil for embankment P1 was on the dry side of optimum compaction water content. Soils on the dry side of optimum tend to erode faster than soils at optimum or slightly wet of optimum compacted water content, according to Hanson and Hunt (2007). The post-breach average dry bulk density and average compacted moisture content for embankment P1 were  $1.79 \text{ g cm}^{-3}$  and  $10.3\%$ , respectively. If plotted on figure 4, the post-breach average dry bulk density and average compacted moisture content for embankment P1 would agree with the laboratory compaction curves.

The series of photos in figure 7 illustrate the process observed during internal erosion of embankment P2. The same procedure used to initiate the internal erosion of embankment P1 was used for each subsequent test. JET analysis

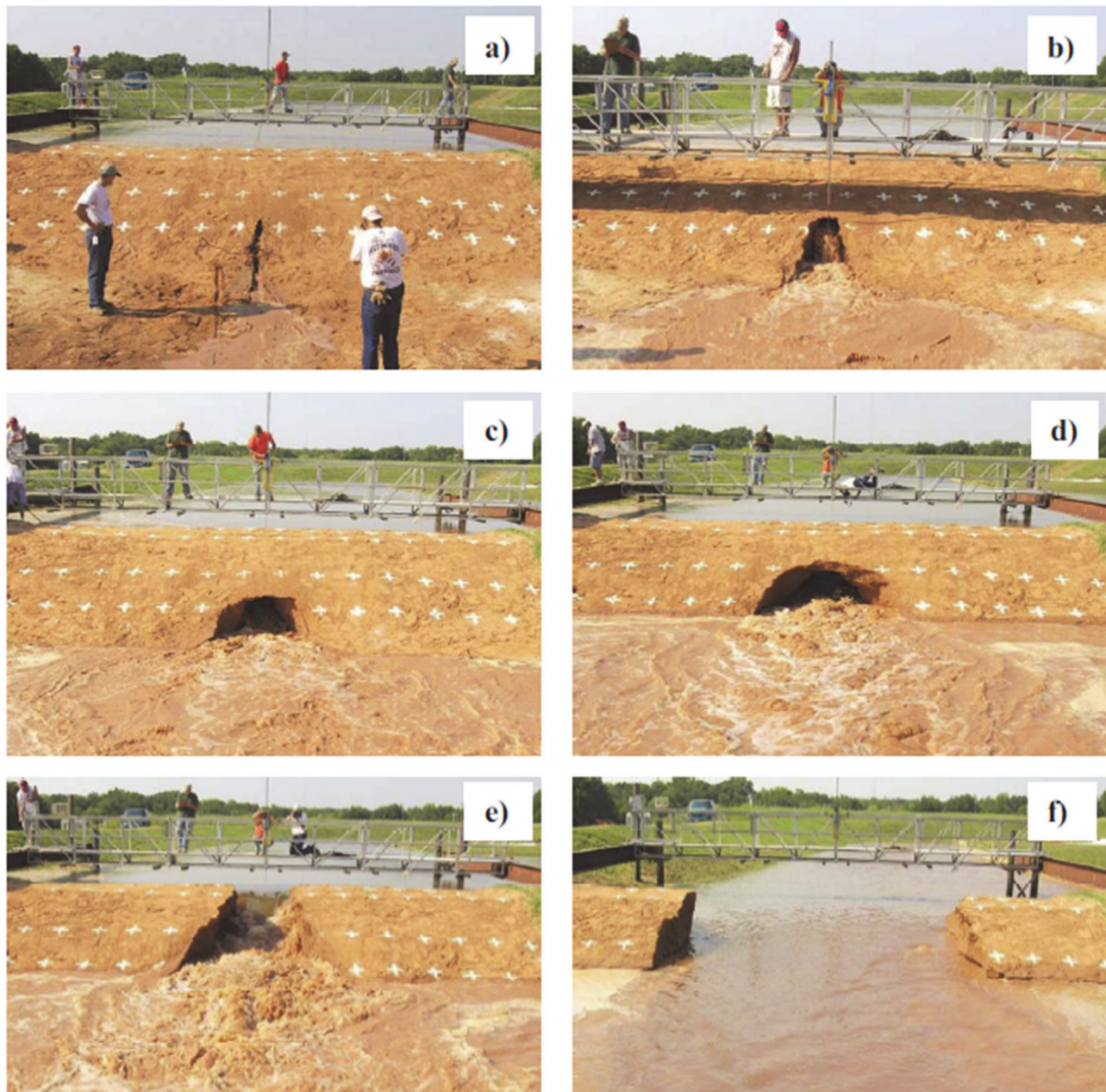
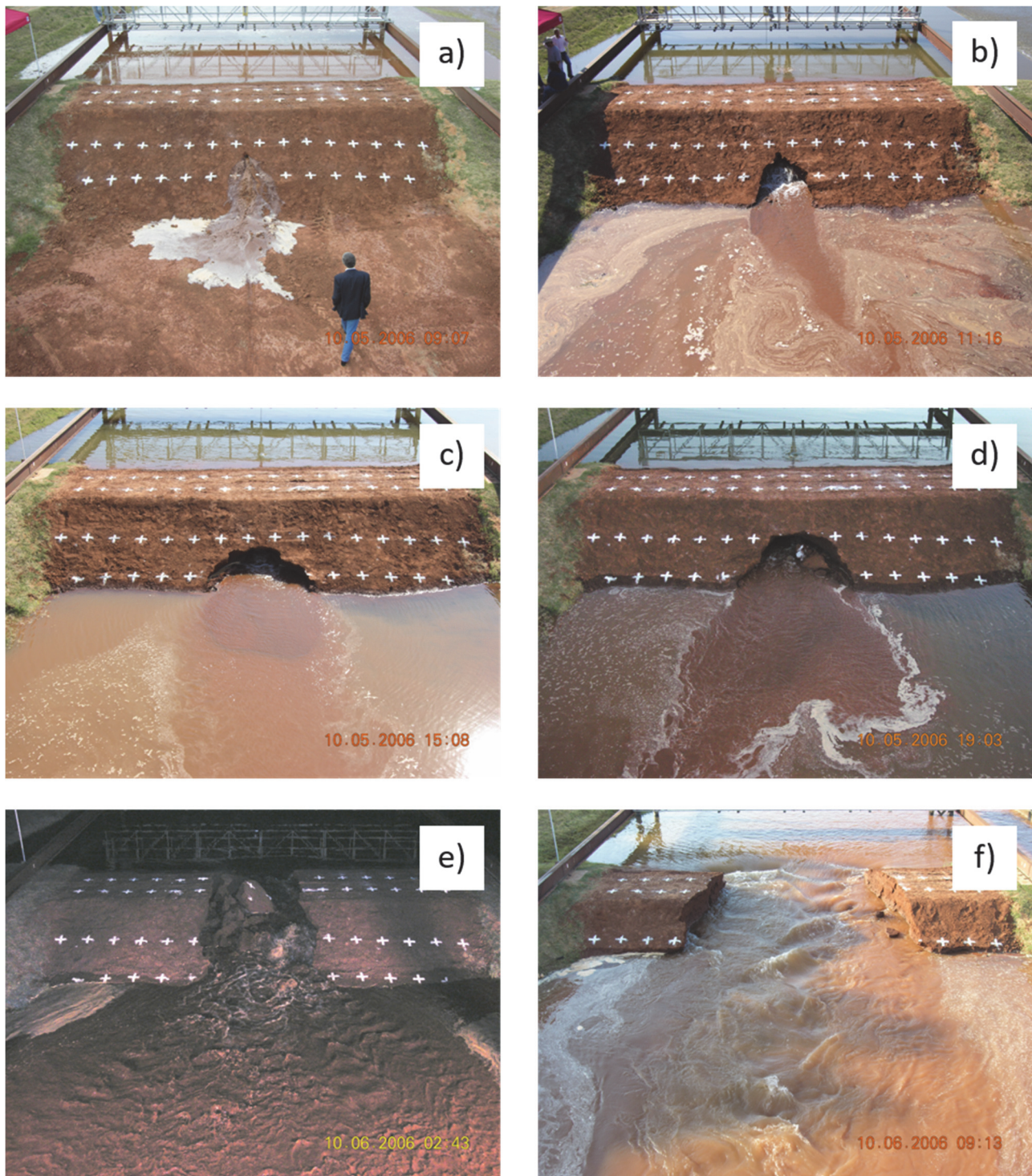


Figure 6. Sequence of internal erosion for test embankment P1: (a) initiation, (b) 6 min, (c) 9 min, (d) 13 min (immediately before collapse), (e) 14 min (immediately following collapse of pipe roof), and (f) 60 min (after Hanson et al., 2010a).

indicated that the  $k_d$  range from the post-breach test was  $0.016 \text{ cm}^3 \text{ N}^{-1} \text{ s}^{-1} \leq k_d \leq 5.3 \text{ cm}^3 \text{ N}^{-1} \text{ s}^{-1}$ . However, the average  $k_d$  for embankment P2 was  $2.4 \text{ cm}^3 \text{ N}^{-1} \text{ s}^{-1}$ , which was consistent with the standard erodibility curve for the soil. This value classifies the soil as very close to group 3, with moderately rapid soil erosion. As shown in figures 7a through 7f, the flow path moderately eroded on the downstream side, with a headcut developing near the flow outlet and progressing upstream internally into the embankment. The average compacted moisture content for P2 from the samples taken during construction was 12.6%, whereas the average compacted moisture content post-breach was 13.1%. The average dry bulk density for P2 also showed slight differences between the construction samples and post-breach measurements. For P2, the construction average and post-breach

average dry bulk densities were  $1.74$  and  $1.83 \text{ g cm}^{-3}$ , respectively. Like P1, the post-breach measurements of average dry bulk density and average compacted moisture content aligned more closely with the compaction curves generated from the laboratory samples. The top of embankment P2 collapsed at approximately 17.5 h into the test. Breach widening continued after the collapse, with the test ending approximately 26.5 h after test initiation.

The series of photos in figure 8 illustrate the process observed during internal erosion of embankment P3. According to table 1, the erosion was expected to be moderately slow (group 4) to moderately rapid (group 3), given the average  $k_d$  of  $0.3 \text{ cm}^3 \text{ N}^{-1} \text{ s}^{-1}$ . The flow path on the downstream side expanded relatively slowly. The top of the embankment collapsed at approximately 20 h into the test. Figure 9



**Figure 7.** Sequence of internal erosion for test embankment P2: (a) initiation, (b) 131 min, (c) 361 min, (d) 536 min, (e) 1056 min (following collapse of pipe roof), and (f) 1595 min, continued widening.

illustrates the erosion process observed for embankment P4. With  $k_d = 0.09 \text{ cm}^3 \text{ N}^{-1} \text{ s}^{-1}$  and erosion group 4 (table 1), erosion was expected to be moderately slow for P4. The flow path on the downstream side expanded very slowly over a period of 72 h and never created a condition for the top of the embankment to collapse. After 72 h, the P4 test was terminated. While embankments P3 and P4 were constructed from soils from the same borrow pit and had similar soil properties (table 2), the erosion process was faster for

embankment P3 than for embankment P4, which coincided with the differences in the average erodibility for P3 and P4, as shown in figure 5. In addition, it was noted during construction of P3 that the soil placement was variable due to hot temperatures, making it difficult to control the compacted water content.

Notes from post-breach *in situ* JETs on the remaining embankment materials for P3 revealed a compacted layer (layer 5) that was noticeably more erodible than the other

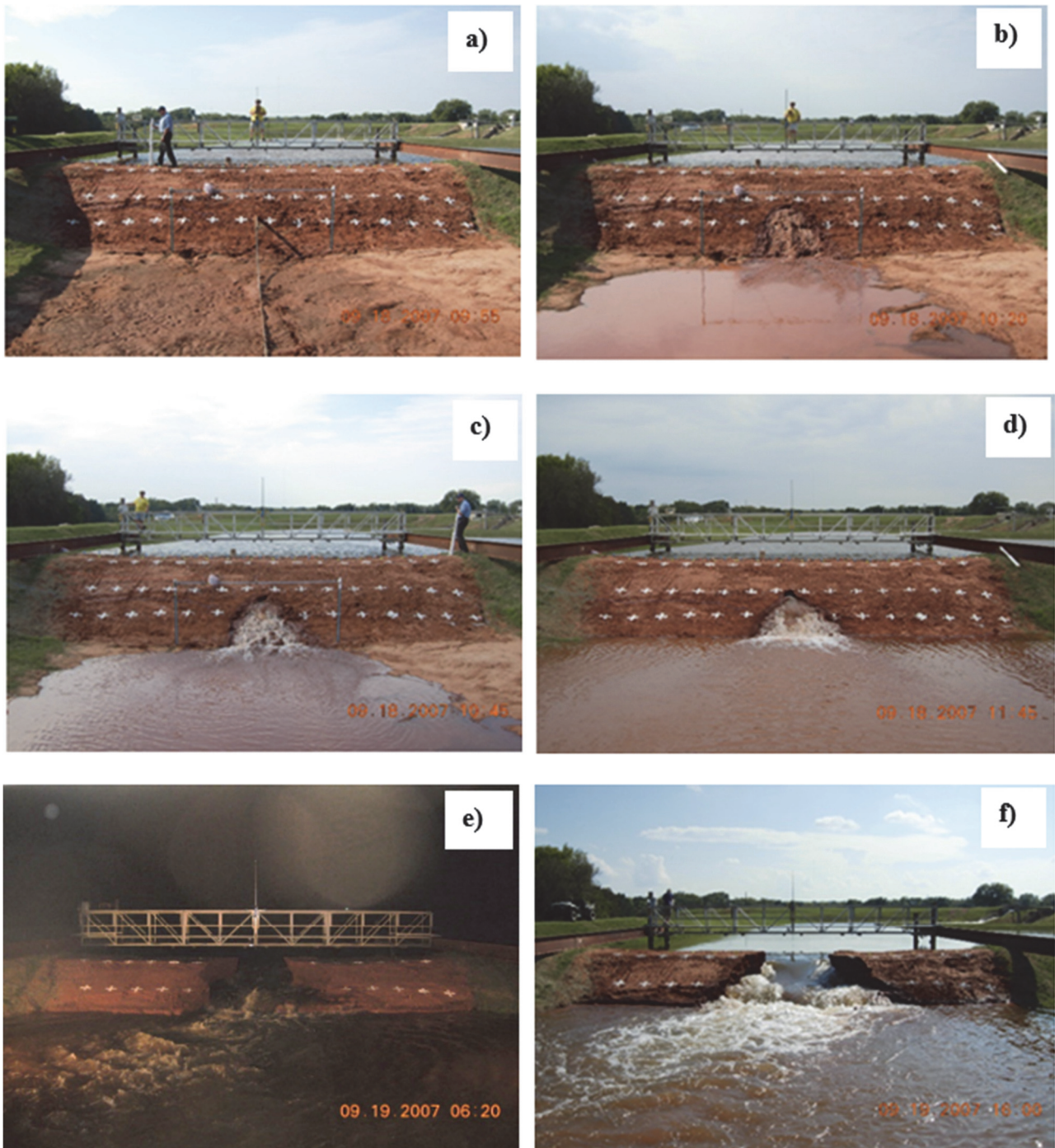


**Figure 8.** Sequence of internal erosion for test embankment P3: (a) time zero prior to pipe removal from the embankment, (b) 18 min, (c) 43 min, (d) 103 min, (e) 1218 min (following collapse of pipe roof), and (f) 1496 min, continued widening.

layers. This layer was near the internal erosion initiation point, the intersection of layers 3 and 4. Therefore, the moisture content at placement for some portions of the embankment likely created more erodible conditions. This was evident in the data, as the variability of the measured  $k_d$  for P3 ( $0.056 \text{ cm}^3 \text{ N}^{-1} \text{ s}^{-1} \leq k_d \leq 1.52 \text{ cm}^3 \text{ N}^{-1} \text{ s}^{-1}$ ) was consistently greater than the variability of the measured  $k_d$  for P4 ( $0.055 \text{ cm}^3 \text{ N}^{-1} \text{ s}^{-1} \leq k_d \leq 0.19 \text{ cm}^3 \text{ N}^{-1} \text{ s}^{-1}$ ). Figure 5 also illustrates that  $k_d$  deviated from the standard erodibility curve for P3 more so than for P4. This test illustrates the importance of soil placement and construction techniques. Quality

assurance during embankment construction is vital, as it can influence the timing of a breach failure. The weakest material along the flow path is preferentially eroded, making it difficult to accurately determine a representative  $k_d$  value for an existing embankment.

Figures 10 through 13 present the inflow, pipe outflow, overflow weir flow, reservoir water elevation, estimated tailwater elevation, and downstream toe erosion width for tests P1, P2, P3, and P4, respectively. As shown in figure 10a, the pipe outflow increased rapidly beginning at about 2 min prior to the pipe (eroding flow path) collapsing 14 min

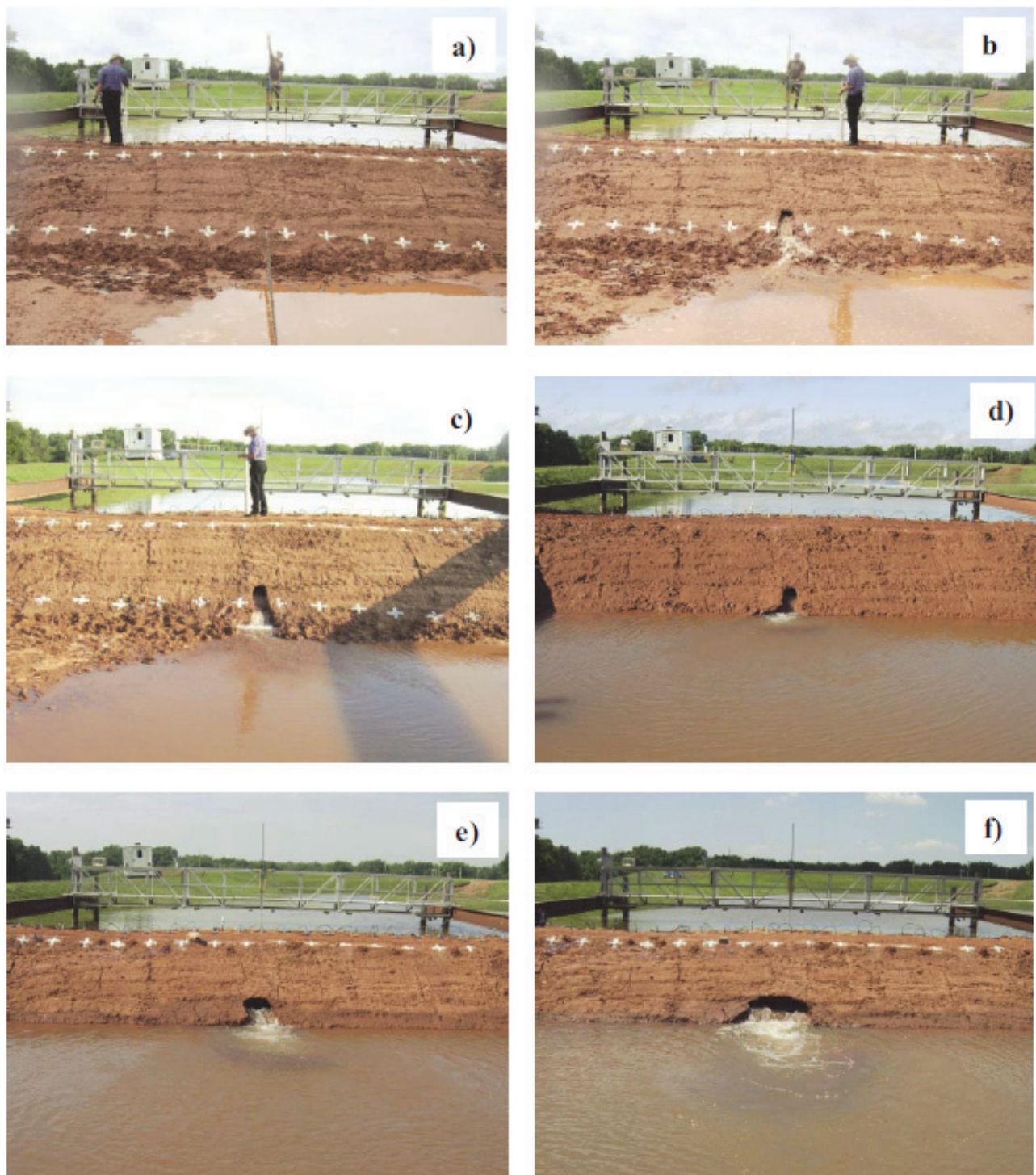


**Figure 9.** Sequence of internal erosion for test embankment P4: (a) time zero prior to pipe removal from the embankment, (b) 15 min, (c) 7 h, (d) 21 h, (e) 46 h, and (f) 72 h (after Hanson et al., 2010a).

after flow initiation and maintained this rate of increasing flow for about 2 min following the collapse. This period of rapid flow rate increase coincided with a transition from orifice to weir control and subsequent breach widening and lowering of the elevation of hydraulic control. This may have been initiated by the arrival of the internal headcut at the upstream end of the pipe. Embankment P2 exhibited similar behavior in the rate of pipe outflow, as shown in figure 11, and this corresponded with top of the dam collapsing

into the breach and the rapid rate of widening thereafter. Erosion widths for each of the tests are identified as the erosion width at or near the downstream (DS) toe of the embankment and the erosion width at the downstream edge of the embankment crest.

Figure 12a shows a steady increase in the rate of pipe outflow for P3, while figure 13a shows a relatively constant to slight increase in pipe outflow for P4. As previously stated, the soils for embankments P3 and P4 came from the same

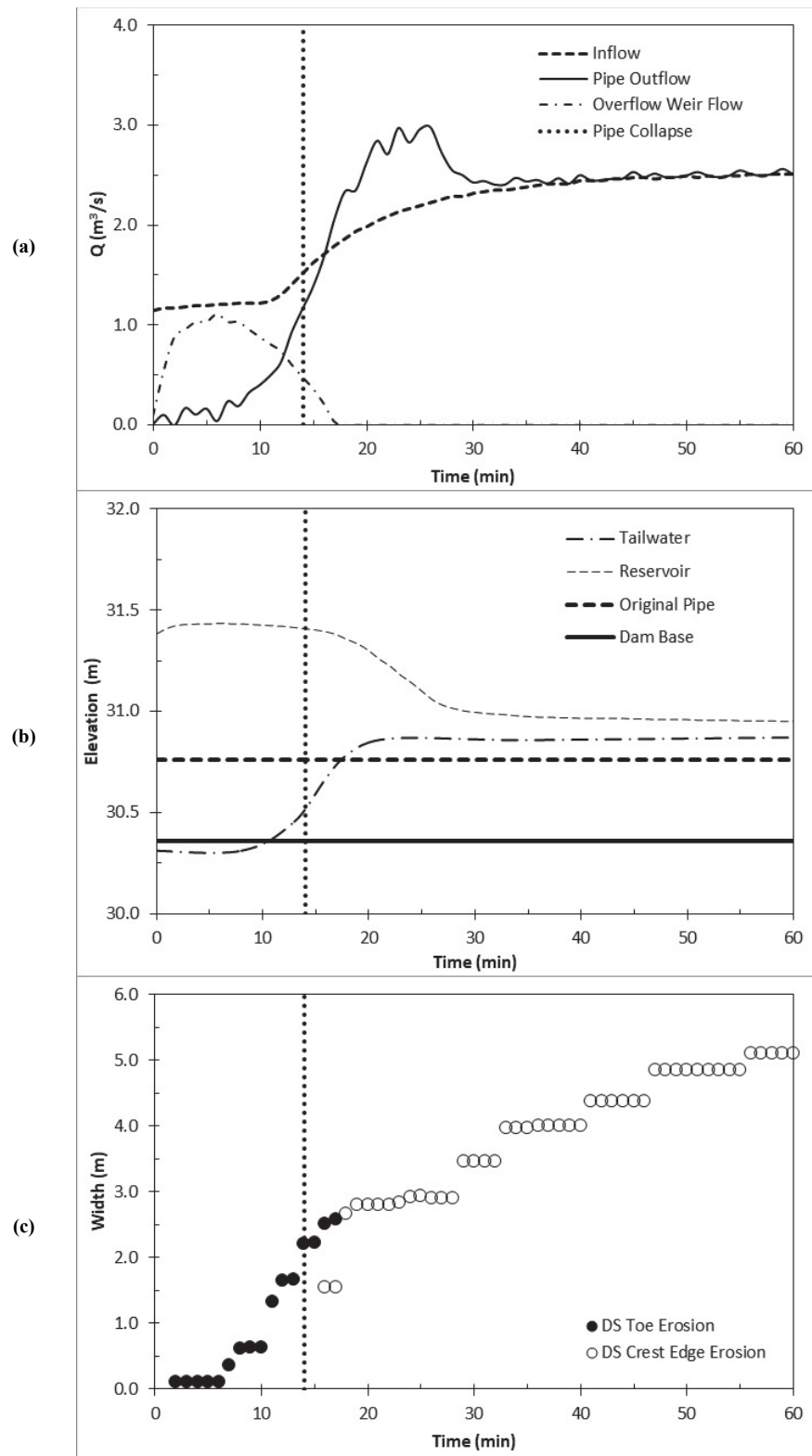


Figure 10. Embankment P1 time series of (a) inflow, pipe outflow, and overflow weir flow discharge ( $Q$ ) through the embankment with internal pipe collapse at 14 min, (b) reservoir, tailwater, original pipe, and dam base elevations, and (c) rate of erosion widening at downstream (DS) embankment toe and crest edge.

borrow pit, yet embankment P3 was constructed with more variability in the compacted moisture content between soil layers than embankment P4. For instance, the construction soil samples for P3 resulted in an average compacted moisture content of 15.3%, while the average compacted

moisture content for the P4 construction soil samples was 17.5%. Post-breach *in situ* JETs indicated that the most erodible construction layer in embankment P3 was lift 5, which was at an elevation near the internal erosion initiation point. In addition, the average post-breach  $k_d$  showed less erosion

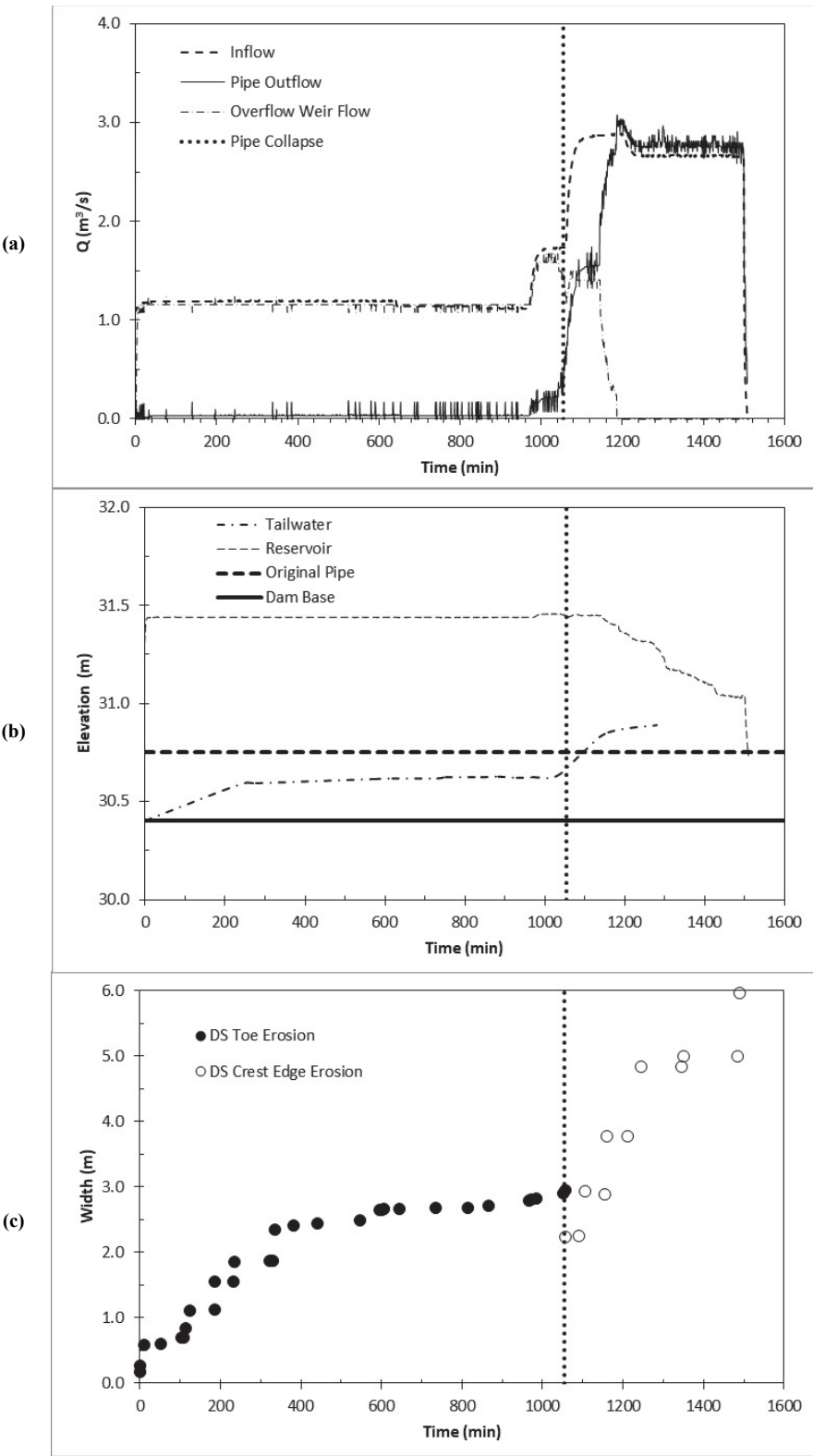


Figure 11. Embankment P2 time series of (a) inflow, pipe outflow, and overflow weir flow discharge ( $Q$ ) through the embankment with internal pipe collapse at 1056 min, (b) reservoir, tailwater, original pipe, and dam base elevations, and (c) rate of erosion widening at downstream (DS) embankment toe and crest edge.

resistance for P3 than for P4. Embankment P4 was more erosion resistant, and the internal flow path did not reach a point of collapsing after 72 h of testing, as illustrated in figure 10 and highlighted in the data shown in figure 13.

The breach widening for embankment P3 did not show any distinctive difference before and after the collapse of the top of the dam, as shown in figure 12c.

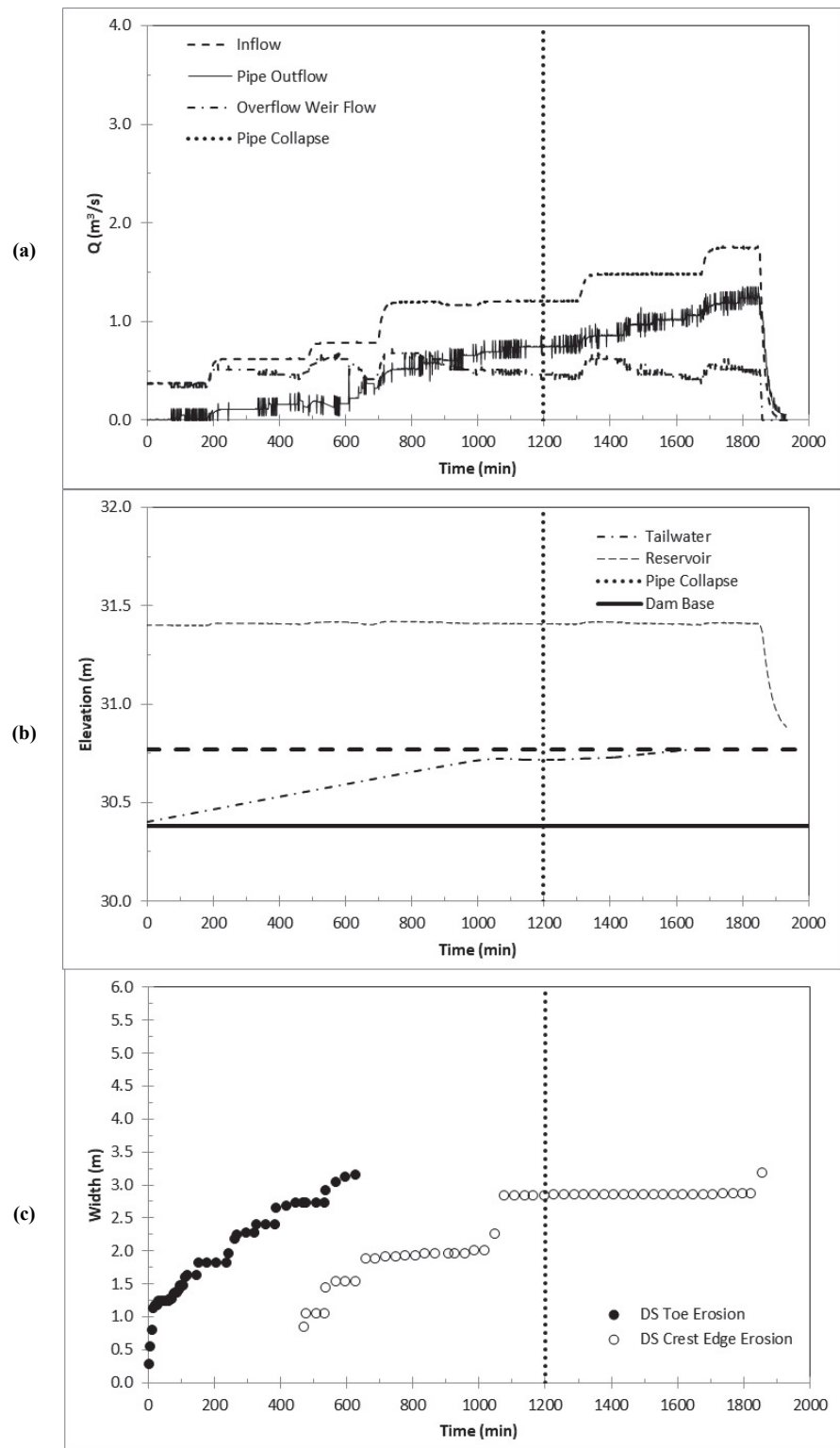


Figure 12. Embankment P3 time series of (a) inflow, pipe outflow, and overflow weir flow discharge ( $Q$ ) through the embankment with internal pipe collapse at 1218 min, (b) reservoir, tailwater, original pipe, and dam base elevations, and (c) rate of erosion widening at downstream (DS) embankment toe and crest edge.

Figures 10 through 13 show significant variability in the pipe outflow. This variability can be attributed to the relative time scale, differences in soil materials, and headcut development and advancement within the eroding flow path. Tailwater did not have any significant influence on the internal erosion process in any of the tests. Figures 6 through 13

indicate distinct contrasts in the performance of the three soils under similar initial internal erosion conditions. For instance, the rate of internal erosion development and the peak discharge increased with increasing erodibility. In addition, the time to collapse of the top of the embankment decreased with increasing erodibility, as shown in figure 14.

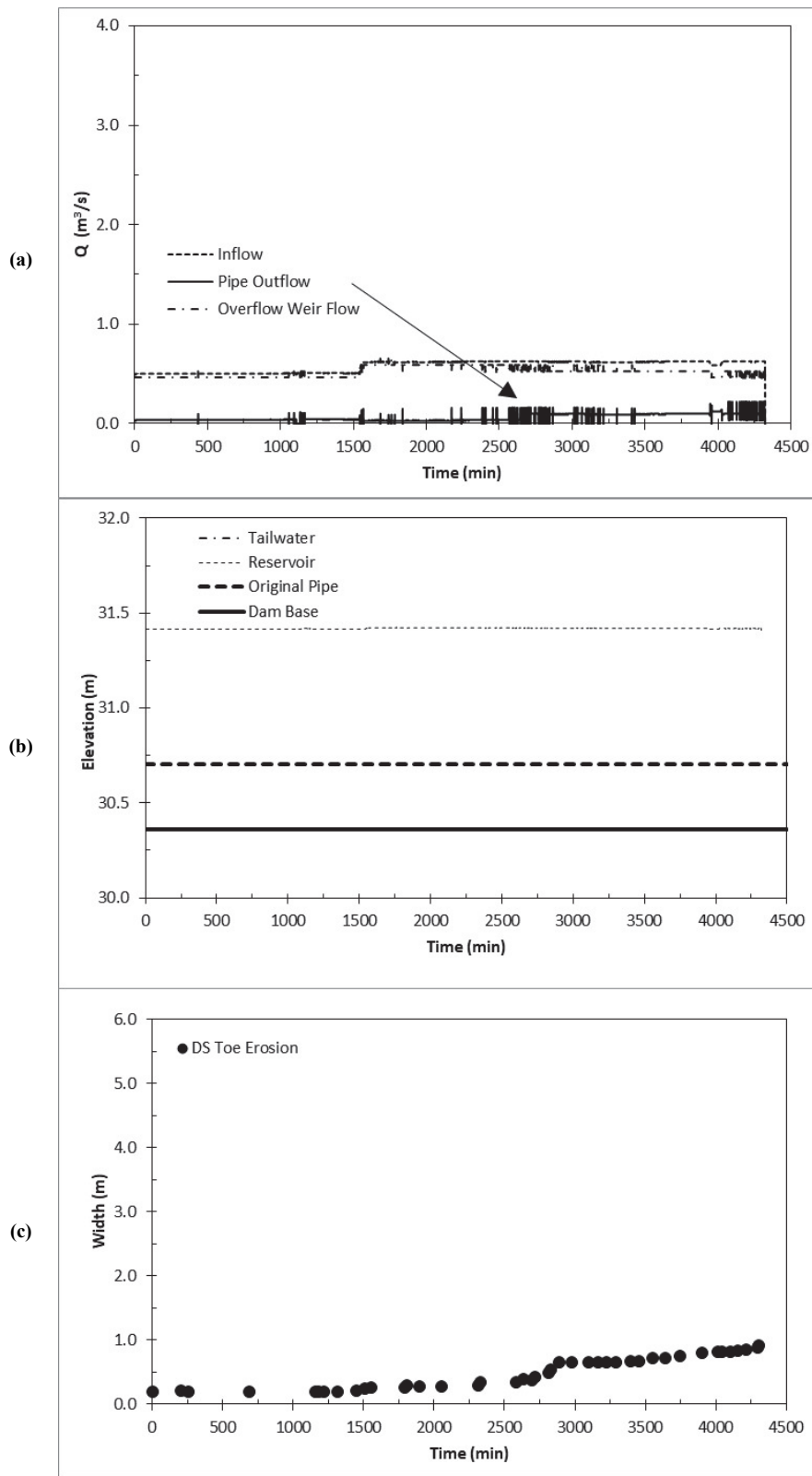


Figure 13. Embankment P4 time series of (a) inflow, overflow weir flow, and outflow discharge ( $Q$ ) through the embankment, (b) reservoir, tailwater, original pipe, and dam base elevations, and (c) rate of erosion widening at downstream (DS) embankment toe.

## SUMMARY AND CONCLUSIONS

This research provides insight into breach development as it pertains to internal erosion, which is one of the most common embankment failure modes. Intermediate-scale

physical tests of homogeneous earthen embankment dams were conducted to simulate internal erosion processes during embankment failure. The internal erosion processes were greatly influenced by the soil properties of the four

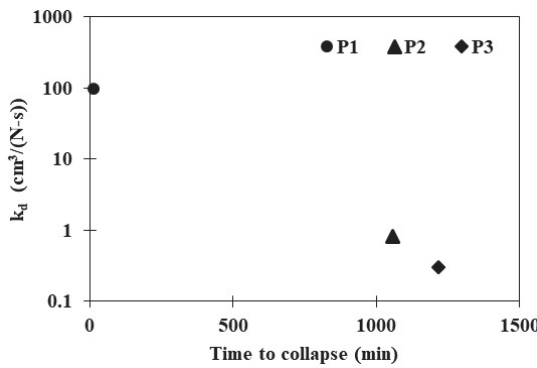


Figure 14. Average post-breach erodibility ( $k_d$ ) versus time to pipe collapse for each test.

tests. Embankment P1 eroded rapidly, and embankment P2 eroded less rapidly in comparison, which was expected given the soil characterization summarized by tables 1 and 2. Embankment P4 exhibited very slow progression in erosion development, which showed agreement with laboratory and *in situ* soil erodibility results. Embankment P3, constructed from the same soil as P4, provided insights into the importance of quality assurance during embankment construction. Variability of the compacted moisture content during the placement of embankment P3 was observed among the lift layers, with one layer noticeably more erodible than the other layers.

Embankment P3 was observed to be more erodible than embankment P4, and its construction during hotter conditions, leading to poor and variable compaction (dry of optimum in some layers), was a likely contributor to this outcome. This compromised the integrity of the embankment and caused it to erode at a rate that was consistent with the erosion resistance of the poorly compacted layers. The variability of this embankment makes it difficult to determine a representative  $k_d$  value. The JET results from small-scale laboratory soil samples prepared at standard compaction effort and the *in situ* tests of the embankments agreed with the expected performance of each embankment. For example, as the erodibility increased, the rate of erosion and resulting peak discharge increased, and the time to collapse for the top of the embankment decreased. Thus, JET results likely provide a basis for predicting the outcomes of actual internal erosion events.

Knowledge gaps still exist in the understanding of the erosion and breach processes of dams and levees, including but not limited to internal erosion due to seepage forces, internal erosion through embankment defects, overtopping erosion of zoned embankments, overtopping erosion that concentrates flow at the embankment intersection with the valley wall (e.g., dam groin), and overtopping erosion impacting stability berms. Better understanding of these components and better capabilities for mapping localized vulnerabilities in embankment dams and levees will enable improvement of embankment erosion and breach models (e.g., WinDAM), which will help inform dam safety policymakers, improve dam failure warning systems, and improve emergency action plans.

## ACKNOWLEDGEMENTS

The authors would like to acknowledge the contributions made to this work by Dr. Greg Hanson and Mr. Darrel Temple, retired research leaders at the USDA-ARS Hydraulic Engineering Research Unit. Their insight and forward thinking in the dam safety community have led to significant improvements in the understanding of the science of embankment breach erosion processes. The authors wish them well in their retirement and dedicate this research in their honor.

## REFERENCES

- Abt, S. R., & Johnson, T. L. (1991). Riprap design for overtopping flow. *J. Hydraul. Engr.*, 117(8), 959-972. [https://doi.org/10.1061/\(ASCE\)0733-9429\(1991\)117:8\(959\)](https://doi.org/10.1061/(ASCE)0733-9429(1991)117:8(959))
- ASTM. (2000a). D2487: Standard practice for classification of soils for engineering purposes (unified soil classification system). West Conshohocken, PA: ASTM.
- ASTM. (2000b). D4318: Standard test methods for liquid limit, plastic limit, and plasticity index of soils.. West Conshohocken, PA: ASTM.
- ASCE Task Committee on Dam/Levee Breaching. (2011). Earthen embankment breaching. *J. Hydraul. Eng.*, 137(12), 1549-1564. [https://doi.org/10.1061/\(ASCE\)HY.1943-7900.0000498](https://doi.org/10.1061/(ASCE)HY.1943-7900.0000498)
- Bernatek-Jakiel, A., & Poesen, J. (2018). Subsurface erosion by soil piping: Significance and research needs. *Earth Sci. Rev.*, 185, 1107-1128. <https://doi.org/10.1016/j.earscirev.2018.08.006>
- Costa, J. E. (1985). Floods from dam failures. USGS Open File Report 85-560. Denver, CO: U.S. Geological Survey.
- Dunker, C. (2019). Flood damage estimate grows to \$1.3 billion; Relief efforts include Nebraska Strong Day. *Lincoln Journal Star* (20 Mar. 2019). Retrieved from [https://journalstar.com/news/local/flood-damage-estimate-grows-to-1-3-billion-relief-efforts-include-nebraska-strong-day/article\\_50888549-d48d-5486-a348-1d6e7c1bd4fc.html](https://journalstar.com/news/local/flood-damage-estimate-grows-to-1-3-billion-relief-efforts-include-nebraska-strong-day/article_50888549-d48d-5486-a348-1d6e7c1bd4fc.html)
- Fell, R., Wan, C. F., Cyganiewicz, J., & Foster, M. (2003). Time for development of internal erosion and piping in embankment dams. *J. Geotech. Geoenvir. Eng.*, 129(4), 307-314. [https://doi.org/10.1061/\(ASCE\)1090-0241\(2003\)129:4\(307\)](https://doi.org/10.1061/(ASCE)1090-0241(2003)129:4(307))
- Foster, M., Fell, R., & Spannagle, M. (2000). The statistics of embankment dam failures and accidents. *Canadian Geotech. J.*, 37(5), 1000-1024. <https://doi.org/10.1139/t00-030>
- Fox, G. A., Felice, R. G., Midgley, T. L., Wilson, G. V., & Al-Madhuchi, A.-S. T. (2014). Laboratory soil piping and internal erosion experiments: Evaluation of a soil piping model for low-compacted soils. *Earth Surface Proc. Landforms*, 39(9), 1137-1145. <https://doi.org/10.1002/esp.3508>
- Fread, D. L. (1988). BREACH: An erosion model for earthen dam failures (Model description and user manual). Silver Spring, MD: National Weather Service.
- Frizzell, K. H., Ruff, J. F., & Mishra, S. (1998). Simplified design guidelines for riprap subjected to overtopping flow. *Proc. Annual ASDSO Meeting*. Lexington, KY: Association of State Dam Safety Officials.
- Hanson, G. J., & Cook, K. R. (2004). Apparatus, test procedures, and analytical methods to measure soil erodibility *in situ*. *Appl. Eng. Agric.*, 20(4), 455-462. <https://doi.org/10.13031/2013.16492>
- Hanson, G. J., & Hunt, S. L. (2007). Lessons learned using laboratory JET method to measure soil erodibility of compacted soils. *Appl. Eng. Agric.*, 23(3), 305-312. <https://doi.org/10.13031/2013.22686>
- Hanson, G. J., & Temple, D. (2002). Performance of bare-earth and vegetated steep channels under long-duration flows. *Trans. ASAE*, 45(3), 695-702. <https://doi.org/10.13031/2013.8831>

- Hanson, G. J., Caldwell, L., Lobrecht, M., McCook, D., Hunt, S. L., & Temple, D. (2007). A look at the engineering challenges of the USDA small watershed program. *Trans. ASABE*, 50(5), 1677-1682. <https://doi.org/10.13031/2013.23959>
- Hanson, G. J., Cook, K. R., & Hunt, S. L. (2005). Physical modeling of overtopping erosion and breach formation of cohesive embankments. *Trans. ASABE*, 48(5), 1783-1794. <https://doi.org/10.13031/2013.20012>
- Hanson, G. J., Tejral, R. D., Hunt, S. L., & Temple, D. M. (2010a). Internal erosion and impact of erosion resistance. *Proc. 30th Annual USSD Conf.* Denver, CO: United States Society on Dams.
- Hanson, G. J., Temple, D. M., Hunt, S. L., & Tejral, R. D. (2011). Development and characterization of soil material parameters for embankment breach. *Appl. Eng. Agric.*, 27(4), 587-595. <https://doi.org/10.13031/2013.38205>
- Hanson, G. J., Wahl, T., Temple, D. M., Hunt, S. L., & Tejral, R. D. (2010b). Erodibility characteristics of embankment materials. *Proc. Annual ASDSO Meeting*. Lexington, KY: Association of State Dam Safety Officials.
- Hassan, M., Morris, M., Hanson, G., & Lakhal, K. (2004). Breach formation: Laboratory and numerical modeling of breach formation. *Proc. Annual ASDSO Meeting*. Lexington, KY: Association of State Dam Safety Officials.
- Hunt, S. L., Hanson, G. J., Cook, K. R., & Kadavy, K. C. (2005). Breach widening observations from earthen embankment tests. *Trans. ASABE*, 48(3), 1115-1120. <https://doi.org/10.13031/2013.18521>
- Jia, Y., & L. Hunt, S. (2016). Development of a CCHE2D embankment break model. *Trans. ASABE*, 59(4), 805-814. <https://doi.org/10.13031/trans.59.11217>
- McCook, D. K. (2004). A comprehensive discussion of piping and internal erosion failure mechanisms. *Proc. Annual ASDSO Meeting*. Lexington, KY: Association of State Dam Safety Officials.
- Midgley, T. L., Fox, G. A., Wilson, G. V., Felice, R., & Heeren, D. (2013). *In situ* soil pipeflow experiments on contrasting streambank soils. *Trans. ASABE*, 56(2), 479-488. <https://doi.org/10.13031/2013.42685>
- Mishra, S. K., & Ruff, J. F. (1998). Riprap design for overtopped embankments. Report prepared for the U.S. Bureau of Reclamation. Retrieved from [https://www.usbr.gov/tsc/techreferences/hydraulics\\_lab/pubs/PA\\_P/PAP-0809.pdf](https://www.usbr.gov/tsc/techreferences/hydraulics_lab/pubs/PA_P/PAP-0809.pdf)
- Moglen, G. E., Hood, K., & Hromadka, T. V. (2019). Examination of multiple predictive approaches for estimating dam breach peak discharges. *J. Hydrol. Eng.*, 24(2), 04018065. [https://doi.org/10.1061/\(ASCE\)HE.1943-5584.0001740](https://doi.org/10.1061/(ASCE)HE.1943-5584.0001740)
- NPDP. (2018). National Performance of Dams Program. Stanford, CA: Stanford University, Department of Civil and Environmental Engineering. Retrieved from <http://npdp.stanford.edu/>
- Robbins, B. A., & Griffiths, D. V. (2018). Internal erosion of embankments: A review and appraisal. *Proc. Rocky Mountain Geo-Conf.* (pp. 61-75). Reston, VA: ASCE. <https://doi.org/10.1061/9780784481936.005>
- Robinson, K. M., Rice, C. E., & Kadavy, K. C. (1998). Design of rock chutes. *Trans. ASAE*, 41(3), 621-626. <https://doi.org/10.13031/2013.17230>
- Sherard, J. L., Decker, R. S., & Ryker, N. (1972). Piping in earth dams of dispersive clay. *Proc. Specialty Conf. on Performance of Earth and Earth-Supported Structures, 1 (Part I)* (pp. 589-626). Reston, VA: ASCE.
- Tabrizi, A. A., Elalfy, E., Elkholly, M., Chaudhry, M. H., & Imran, J. (2017). Effects of compaction on embankment breach due to overtopping. *J. Hydraul. Res.*, 55(2), 236-247. <https://doi.org/10.1080/00221686.2016.1238014>
- Temple, D. M. (1985). Stability of grass-lined channels following mowing. *Trans. ASAE*, 28(3), 750-754. <https://doi.org/10.13031/2013.32332>
- Vaskinn, K. A., Løvoll, A., Höeg, K., Morris, M., Hanson, G. J., & Hassan, M. A. A. M. (2004). Physical modeling of breach formation large-scale field tests. *Proc. Annual ASDSO Meeting*. Lexington, KY: Association of State Dam Safety Officials.
- Wahl, T., & Lentz, D. (2011). Physical hydraulic modeling of canal breaches. Report HL-2011-09. Denver, CO: U.S. Bureau of Reclamation Hydraulic Laboratory.
- Wan, C. F., & Fell, R. (2004). Investigation of rate of erosion of soils in embankment dams. *J. Geotech. Geoenvir. Eng.*, 130(4), 373-380. [https://doi.org/10.1061/\(ASCE\)1090-0241\(2004\)130:4\(373\)](https://doi.org/10.1061/(ASCE)1090-0241(2004)130:4(373))
- Wanger, M., Fox, G. A., Wilson, G. V., & Nieber, J. (2019). Laboratory experiments on the removal of soil plugs during soil piping and internal erosion. *Trans. ASABE*, 62(1), 83-93. <https://doi.org/10.13031/trans.13092>
- Wilson, G. (2011). Understanding soil-pipe flow and its role in ephemeral gully erosion. *Hydrolog. Proc.*, 25(15), 2354-2364. <https://doi.org/10.1002/hyp.7998>
- Wilson, G. V. (2009). Mechanisms of ephemeral gully erosion caused by constant flow through a continuous soil pipe. *Earth Surface Proc. Landforms*, 34(14), 1858-1866. <https://doi.org/10.1002/esp.1869>
- Wilson, G. V., & Fox, G. A. (2013). Pore-water pressures associated with clogging of soil pipes: Numerical analysis of laboratory experiments. *SSSA J.*, 77(4), 1168-1181. <https://doi.org/10.2136/sssaj2012.0416>
- Wilson, G. V., Wells, R., Kuhnle, R., Fox, G., & Nieber, J. (2018). Sediment detachment and transport processes associated with internal erosion of soil pipes. *Earth Surface Proc. Landforms*, 43(1), 45-63. <https://doi.org/10.1002/esp.4147>
- Zhong, Q. M., Chen, S. S., Deng, Z., & Mei, S. A. (2019). Prediction of overtopping-induced breach process of cohesive dams. *J. Geotech. Geoenvir. Eng.*, 145(5), 04019012. [https://doi.org/10.1061/\(ASCE\)GT.1943-5606.0002035](https://doi.org/10.1061/(ASCE)GT.1943-5606.0002035)